Available online at www.sciencedirect.com
SCIENCE DIRECT
Journal of Molecular Catalysis A: Chemical 252 (2006) 76–84
JOURNAL OF MOLECULAR CATALYSIS A: CHEMICAL
www.elsevier.com/locate/molcata

Synthesis of nanocrystalline zeolite beta in supercritical fluids, characterization and catalytic activity

M. Lakshmi Kantam [a,*], Bhavnari P.C. Rao [a], B.M. Choudary [b,**], K. Koteswara Rao [a], Bojja Sreedhar [a], Yasuhiro Iwasawa [c], Takehiko Sasaki [c]

[a] *Inorganic and Physical Chemistry Division, Indian Institute of Chemical Technology, Hyderabad 500007, India*
[b] *Ogene Systems (I) Pvt. Ltd. #11-6-56, GSR Estates, Moosapet, Hyderabad 500037, India*
[c] *Department of Chemistry, Graduate School of Science, The University of Tokyo, Bunkyo-Ku Tokyo 113-0033, Japan*

Received 15 October 2005; received in revised form 5 February 2006; accepted 6 February 2006
Available online 23 March 2006

Abstract

Nanocrystalline zeolite beta with Si/Al ratios 12.5–50 has been synthesized by applying a two-stage varying temperature synthesis and supercritical fluid aided crystallization. Low temperature nucleation of clear aluminosilicate gel and SCF aided crystallization gave quantitative yields of nanocrystalline zeolite beta in shorter crystallization time without the use of alkali cations and seeded gel. The obtained nanocrystalline zeolite beta catalysts are thoroughly characterized by X-ray diffraction, N_2 adsorption, ^{29}Si and ^{27}Al MAS NMR, IR spectroscopy and Al incorporation in framework was studied by XPS. These nanocrystalline zeolite beta catalysts displayed good activity and high selectivity towards 4-nitro-*o*-xylene in the nitration of *o*-xylene when compared to microcrystalline zeolite beta.

Keywords: Nanocrystalline zeolite beta; Supercritical fluids; Crystallization time; Nitration; *o*-Xylene; *para*-Selectivity

1. Introduction

The increasing demand of new chemical processes has led to a growing need of highly active and selective catalysts. Nanotechnology is considered a serious option to meet the expectation [1–3]. Crystal size in nanocrystalline materials is reduced to a few unit cells. This leads to the presence of large number of atoms/ions located at the edges and on the surface, which provide inturn a number of active sites for catalyzing the surface reactions. Selectivity also increases due to reduced diffusion limitations [3]. Zeolite beta a three-dimensional large pore aluminosilicate is developing into a major catalyst in organic chemicals conversion, contributing to low waste technology [4]. Nanocrystalline zeolite beta has received much attention in the catalytic applications, when compared to ordinary microcrystalline zeolite beta, because of its higher activity, selectivity and minimal catalyst decay [5–7].

Numerous reports of zeolite crystallization exist in the literature and the key factors in controlling the crystal size are the crystallization conditions such as temperature, stirring, seeding, gel aging and composition-dependent parameters such as alkalinity, dilution, ratio between Si and tetrahedron forming elements, template concentration, ionic strength, presence of crystallization poisons [8]. Nanocrystalline zeolites A, X, ZSM-5 and beta [9–13] are prepared by changing the compositional or crystallization parameters. Nanocrystalline zeolite beta, which was synthesized based on dry gel conversion method in specially designed autoclave in presence of alkali metal cations needs post-treatment to generate acidic sites [12]. On the other hand, in the synthesis of nanocrystalline zeolite beta [13] in absence of alkali metals, the crystallization efficiency on the basis of silicon is low even after longer crystallization times.

Supercritical fluids (SCFs) offer a series of technical advantages in separation technology and chemical engineering [14] because of their unique solubility and diffusivity properties. Proper use of these supercritical fluids in heterogeneous catalysis can afford enhancement of rate of reaction and process intensification in catalyst preparation [15]. Nanocrystalline porous metal

* Corresponding author. Tel.: +91 40 27193510; fax: +91 40 27160921.
** Corresponding author. Tel.: +91 40 23775566; fax: +91 40 23775566.
E-mail addresses: lkmannepalli@yahoo.com (M.L. Kantam), bmchoudary@gmail.com (B.M. Choudary).

1381-1169/$ – see front matter © 2006 Elsevier B.V. All rights reserved.
doi:10.1016/j.molcata.2006.02.044

oxides are prepared from drying of hydrolyzed gels in presence of supercritical fluids [16]. It was also found that supercritical fluids are ideally suited for rapid transport of Al into mesoporous silicates to achieve homogeneous Al dispersion [17] and enhancing the rate of deposition of silane based self-assembled monolayers onto mesoporous silicates due to their low viscosity and high diffusivity [18]. Therefore, we hypothesized that supercritical fluid enhance the rate of crystallization and ease the separation to provide finely homogenized crystalline zeolite beta with quantitative yields. We herein report a novel approach for the synthesis of nanocrystalline zeolite beta with different Si/Al ratios in quantitative yields and in about 2 days by modifying nucleation and effecting hydrothermal as well as supercritical fluid aided crystallization. These catalysts display good conversions and high selectivity towards 4-nitro-*o*-xylene in the nitration of *o*-xylene, which is an important intermediate in the synthesis of riboflavin.

2. Experimental

2.1. General

The raw materials used were TEOS (tetraethylorthosilicate, 98%, Aldrich), TEAOH (tetraethylammonium hydroxide, 35 wt% in water, Aldrich), $Al(NO_3)_3{\cdot}9H_2O$ (Aldrich) and deionized water. Other chemicals used were *o*-xylene (S.D. Fine Chem. Ltd.), HNO_3 (70%, S.D. Fine Chem. Ltd.), dichloroethane (S.D. Fine Chem. Ltd.). Commercial (microcrystalline) zeolite beta catalysts were obtained from Zeolyst International.

2.2. Preparation of nanocrystalline zeolite beta

Nanocrystalline zeolite beta catalysts A, B, C, D are synthesized with the compositions of $Al_2O_3{:}xSiO_2{:}(0.26x+1)$ $TEA_2O{:}15xH_2O$, where x values are 25, 30, 50 and 100, respectively. A solution containing aluminum nitrate in 35% aqueous solution of TEAOH was added drop wise to TEOS under stirring at room temperature for 30 min to form a clear gel. Evaporation of ethanol formed during hydrolysis results into a viscous gel, which was aged under stirring at room temperature for 24 h. Hydrothermal treatment of the nucleated gel was carried out in stainless steel autoclave for 24 h at 130 °C to obtain white colloidal suspension. To this colloidal suspension, a mixture of methanol and toluene was added in 1:1 ratio (the solvent to gel ratio is 4.0–4.3) and then flushed with N_2 gas. The reactor was pressurized with N_2 gas up to 150 psi and heated to 265 °C by raising the temperature slowly 1 °C/min and kept at this temperature for 10 min. The solvent vapor was vented at this temperature by controlled evaporation within 1 min. The reactor was removed immediately from the heater, flushed with N_2 gas for about 5 min, allowed to cool to room temperature to obtain nanocrystalline zeolite beta. Nanocrystalline zeolite beta was dried in an oven at 120 °C for 12 h and calcined in a flow of air at 600 °C for 6 h to remove organic template molecules.

2.3. Characterizations

The crystallinity and phase purity of the solids were determined by powder X-ray diffraction (XRD) using a Siemens D5000 diffractometer and Cu Kα radiation. The IR spectra for the framework vibration were recorded on a Nicolet–740 instrument with a resolution of 4 cm^{-1} using KBr wafer technique. The content of aluminum of the crystallization products was measured by atomic absorption spectroscopy (Perkin Elmer AAanalyst 300). The amount of Silicon was measured by conventional gravimetric analysis. CHN analyses were performed by Elementar Vario EL (Germany) instrument. N_2 physisorption was carried out at 77 K on Autosorb-1 (Quantachrome, USA) instrument. The catalysts were outgassed in vacuum at 250 °C for 12 h before measurement. The surface area was estimated according to BET equation and micropore volume was obtained by *t*-plot method. TGA–MS thermograms were recorded on a Mettler–Toledo TGA/SDTA 821e instrument coupled to a Blazers Thermostar GSD300T in the temperature range 25–700 °C with heating rate of 10 °C/min in a air atmosphere.

MAS NMR spectra were recorded on a Chemagnetics CMX-300 spectrometer operating at 59.68 MHz for ^{29}Si and 78.17 MHz for ^{27}Al. In both cases single pulse detection method with hydrogen decoupling was used, where the pulse duration was 1.5 μs (corresponding to about $\pi/6$ pulse). For ^{29}Si MAS NMR spectra, the rotor spin rate was 4 kHz, with a delay time of 20 s and 2000 transients were accumulated. Tetramethylsilane (TMS), fused in a glass tube was used as an external reference (0 ppm). For ^{27}Al, 0.1 M solution of $Al(NO_3){\cdot}6H_2O$ was used as the external reference (0 ppm), with a rotor spin rate of 4 kHz and a delay time was 30 s. The number of transients recorded were 2000. Deconvolution into gaussian peaks was performed to obtain site-resolved ^{29}Si NMR peak intensities corresponding to the Q1(1Al) site, Q0(5-membered ring) and Q0(4-membered ring). Deconvoluted curves and the sum of them were completely in agreement with the original spectra. The ^{13}C MAS CP (cross polarization) NMR spectra were also recorded on a Chemagnetics CMX-300 spectrometer operating at 75.54 MHz for ^{13}C and 300.44 MHz for ^{1}H with MAS rate of 4 kHz. The ^{1}H 90° pulse width was 3.65 μs and the contact time was 5 ms. Proton decoupling was adopted during recording FID. The pulse delay was 30 s and the typical accumulation number was 7000. Chemical shifts were referred to external adamantane that exhibits two peaks at 37.9 and 28.5 ppm with respect to tetramethylsilane (TMS). TEM images of the samples were recorded on a PHILIPS make TECNAI 12 FEI TEM instrument. The samples were suspended in distilled water and treated with ultrasound for 30 min. One drop of the sample was kept on to a Formvar coated copper grid, dried and recorded the TEM images. The operated voltage was 100 kV.

XPS spectra were recorded on a KRATOS AXIS 165 with a dual anode (Mg and Al) apparatus using the Mg Kα anode. The pressure in the spectrometer was about 10^{-9} Torr. For energy calibration the carbon 1s photoelectron line was used. The carbon 1s binding energy was taken to be 285.0 eV. Spectra were deconvoluted using Sun Solaris based Vision 2 curve resolver. The location and the full-width at half maximum (FWHM) for a

species was first determined using the spectrum of a pure sample. The location and FWHM of products, which were not obtained as pure species, were adjusted until the best fit was obtained. Symmetric Gaussian shapes were used in all cases. Binding energies for identical samples were, in general, reproducible to within ±0.1 eV.

The measurements of temperature-programmed disorption of ammonia (NH_3-TPD) were carried out using a Sorbstar-200 instrument. After activating the sample (400 mg) at 400 °C in a flow of argon (50 ml min^{-1}) for 4 h, followed by cooling to room temperature, gaseous ammonia (1 vol% in argon) was passed over the activated sample for 1 h. Loosely bound ammonia was removed by purging the catalyst with pure argon for 1 h. Then the sample was heated from 150 to 700 °C with a ramp of 10 °C min^{-1} while monitoring the evolved ammonia concentration using thermal conductivity and mass spectrometric detectors.

2.4. Catalytic tests

In a typical reaction, 1.06 g (10 mmol) of *o*-xylene and 0.1 g of the dried catalyst (120 °C, overnight) were taken in a 50-ml two-necked round-bottomed flask along with 6 ml of dichloroethane as the solvent. The resulting mixture was heated to 85 °C and when the steady state was acquired, 1.06 g (12 mmol) of nitric acid (70%) was slowly added for 1 h and continued the reaction for 5 h. A reverse Dean-Stark apparatus was used to separate water formed during the reaction. After completion of the reaction, the reaction mixture was filtered and the filtrate was subjected to base wash to remove the excess acid. The products were analyzed in a gas chromatograph (HP 6890) equipped with a flame ionization detector (FID) and a capillary column (HP-1 fused silica). The products were also identified by GC–MS (Agilent 6890) analysis. Calibration of GC peak areas was carried out by taking solutions of known compositions. The conversion was calculated on the basis of weight percent of substrate. The initial weight percent of *o*-xylene was divided by initial area percent (*o*-xylene peak percent from GC) to get the response factor. The unreacted weight of *o*-xylene was calculated by multiplying response factor with the area percentage of the GC peak for *o*-xylene obtained after the reaction. The conversion and selectivity of was calculated as follows:

$$\text{Conversion (wt\%)} = \frac{\text{initial wt\%} - \text{final wt\%}}{\text{initial wt\%}} \times 100$$

$$\text{Selectivity of 4-nitro-}o\text{-xylene (\%)} = \frac{\text{GC peak area of 4-nitro-}o\text{-xylene}}{\text{sum of the GC peak area of all products}} \times 100$$

Recycling of the catalyst was done by following the procedure: (i) separation from the reaction mixture by filtration, (ii) thorough washing with dichloroethane (20 ml), (iii) drying at 110 °C for 2 h and (iv) activation at 450 °C for 2 h in air.

3. Results and discussion

3.1. Synthesis of nanocrystalline zeolite beta

Fig. 1 shows the evolution of nanocrystalline zeolite beta containing Si/Al ratio = 15 through various stages of transformation right from gel to zeolite by TEM images. Controlled addition of

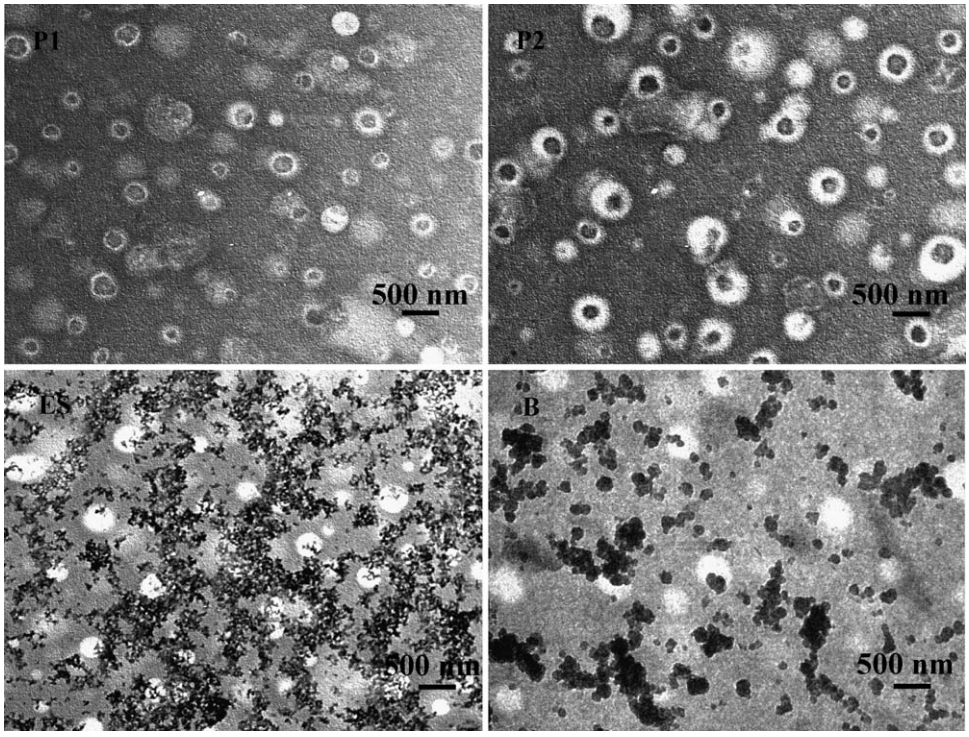

Fig. 1. TEM images of nanocrystalline zeolite beta (Si/Al ratio = 15) during the synthesis: (P1) hydrolyzed gel, (P2) nucleated gel after 24 h, (ES) extended structures and (B) nanocrystalline zeolite beta.

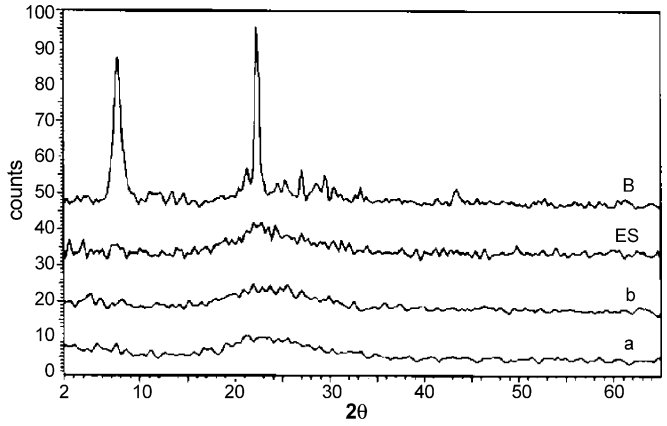

Fig. 2. XRD patterns of nanocrystalline zeolite beta (Si/Al ratio = 15) obtained by applying different conditions: (a and b) SCF aided crystallization of nucleated gel for 10 min and 12 h, respectively, (ES) without SCF aided crystallization and (B) hydrothermal treatment coupled with SCF aided crystallization.

aluminate solution to silica source and evaporation of ethanol formed during hydrolysis yields reactive hydrolyzed gel. Low temperature aging (nucleation) of this hydrolyzed gel forms silicate and aluminate monomers required for the building blocks of zeolite beta nuclei. The samples P1 and P2 are hydrolyzed gel and nucleated gel respectively show the aluminosilicate gel particles. IR spectrum of the sample P2 shows the absorption band at 550 cm^{-1}, which confirms the formation of 5-membered ring subunits of zeolite nuclei [19]. Hydrothermal treatment of nucleated gel for 24 h gives the aluminosilicate nanoparticles (Fig. 1 ES). XRD spectrum of this sample is amorphous (Fig. 2 ES) and IR spectrum of the sample has shown similar absorption bands to that of intermediate structure of zeolite beta [20]. The ^{29}Si NMR spectrum of this sample has shown broad resonance bands centered at −89.7, −100.4 and −109 ppm, these resonance bands indicate the presence of $Si(OH)_2$ defect groups, Si(1Al) and Si(0Al) sites, respectively [21,22] and ^{27}Al NMR spectrum of this sample reveals that Al is in tetrahedral coordination. These data indicate the presence of extended structures of zeolite beta. Finally SCF aided crystallization and depressurization of the supercritical fluids in short period allow the formation of free flow powder of nanocrystalline zeolite beta (B) (Figs. 1 and 2).

TEOS and aluminum nitrate or aluminum sulfate have been used as silica and aluminum sources as these compounds form highly reactive gels and evaporation of ethanol formed during hydrolysis aids a faster nucleation from gel during aging [23,24]. It has been widely accepted that aging of hydrolyzed gel at ambient temperature decreases the duration of crystallization and crystal size [25,26] but zeolite beta is known to crystallize at higher temperature only [27]. So we applied a two-stage varying temperature synthesis for both nucleation and crystallization steps. It has also been reported that the absence of alkali cations in the synthesis of nanocrystalline zeolite beta greatly effects the crystallization kinetics and complete crystallization will occur after longer crystallization time [13]. As enumerated the above advantages in the use of supercritical fluids, we studied the effect of supercritical fluids to synthesize the nanocrystalline zeolite beta in shorter crystallization time. The samples subjected to direct SCF aided crystallization of the nucleated gel by using a mixture of hydrophobic and hydrophilic solvent for about 10 min and 12 h, respectively (Fig. 2a and b) yield amorphous product. The application of SCF aided crystallization to the sample obtained after 24 h of hydrothermal treatment of nucleated gel at 130 °C results nanocrystalline zeolite beta in high purity and in quantitative yield. To substantiate the effect of SCF step in the crystallization of zeolite beta, we have conducted controlled reaction subjecting the hydrothermally treated nucleated gel for 24 h at 130 °C to the high temperature used in SCF step (130–265 °C) without SCFs. Table 1 listed the physicochemical properties of high temperature treated extended structures of zeolite beta (HT 15 and HT 50) and nanocrystalline zeolite beta catalysts obtained by SCF aided crystallization (A–D). The Si/Al ratio of the initial gel and obtained zeolite were well matched

Table 1
Physicochemical characteristics of the nanocrystalline zeolite beta catalysts

	HT 15	HT 50	A	B	C	D
Si/Al ratio						
Gel	15.0	50.0	12.5	15.0	25.0	50.0
Zeolite	10.0	19.7	12.5	15.0	25.0	50.0
Yield (%)[a]	68.08	57.10	98.75	98.65	96.88	96.75
XRD crystallinity (%)	40	Am	100[b]	100	84	70
Surface area (m^2/g)	381.8	116.4	515.3	493.6	433.0	425.0
Micropore volume (cm^3/g)[c]	0.0694	−0.003	0.1979	0.1759	0.1429	0.1438
Crystal size (nm)[d]	>200	–	40–80	60–80	70–80	80–90
Si/Al ratio (XPS)	9.35	15.94	10.89	17.45	26.20	52.45
Binding energies (eV)						
Si 2p	103.5	103.7	103.6	103.6	103.5	102.2
Al 2p	74.1	74.9	74.7	74.5	74.5	75.4
α^1 (eV)[e]	–	–	1460.3	1460.3	1460.1	1460.5
Acidity TPAD (mmol/g)	–	–	0.782	0.562	0.473	0.349

[a] Yields are calculated from the weight of nanocrystalline zeolite beta obtained as a proportion of the total weight of SiO_2 and Al_2O_3 initially present in the gel.
[b] Reference zeolite and crystallinity is calculated from the intensity of the most intense (302) reflection peak appearing at 22.4°.
[c] From the *t*-plot.
[d] Estimated from TEM images.
[e] The modified auger parameter (α^1) obtained from the sum of the binding energies of Al 2p and kinetic energy of photoelectron resulting from Al KLL peak.

for the samples A–D whereas large difference is observed in the samples HT 15 and HT 50. The yields of the samples A–D are high when compared to the samples HT 15 and HT 50. The XRD crystallinity of the sample HT 15 is low when compared with the sample obtained by SCF aided crystallization (B) and TEM image of the sample HT 15 shows large particles. Moreover amorphous product is formed for the sample HT 50. The samples (A–D) shows high surface area and micropore volume values whereas the samples HT 15 and HT 50 are not. This indicates that the hydrothermal treatment is important to initiate the crystallization, while SCF aided crystallization increases the rate of crystallization by rapid transportation of aluminosilicate nanoparticles into fully crystalline zeolite beta to give quantitative yields. The absence of SCFs and high temperature treated extended structures yield non-porous large particles with low crystallinity and low yields.

The unique properties of fluids just above the critical point can be applied beneficially in various ways in heterogeneous catalysis. To the best of our knowledge this report represents the first use of SCFs to prepare the nanocrystalline zeolite beta. The enhancement of rate of the crystallization of zeolite beta can be attributed to the fact that the SCF crystallization is carried out at significantly higher pressure than the regular hydrothermal crystallization. An associative process will have a negative $\Delta v^{\ddagger}$ and Δv° (volume of activation and volume of reaction, respectively) associated with it, and increasing the reaction pressure will accelerate such a process as well as drive any equilibrium toward the adduct [28]. The synthesis of zeolite beta is the culmination of nucleation and crystal growth. These processes are associative processes and are therefore expected to accelerate with the increased process pressure.

3.2. Characterization of nanocrystalline zeolite beta

XRD powder patterns of the calcined samples of nanocrystalline zeolite beta (A–D) are presented in Fig. 3. All samples exhibited the typical pattern of highly crystalline zeolite beta with broad and sharp reflections [20] and no other phase impurities were observed. Relative crystallinity is calculated from

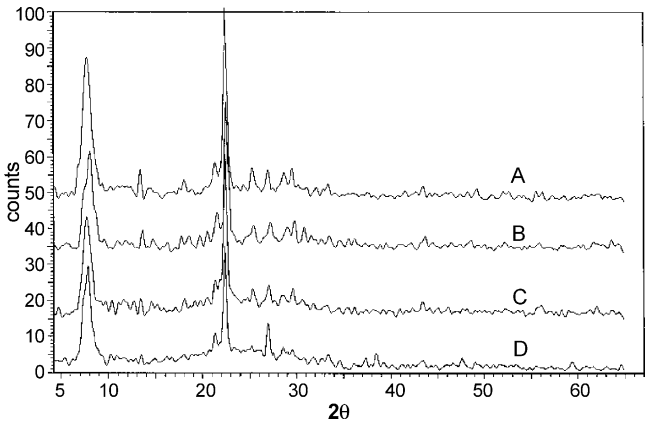

Fig. 3. XRD powder patterns of the calcined samples of nanocrystalline zeolite beta catalysts containing different Si/Al ratios: (A) 12.5, (B) 15.0, (C) 25.0 and (D) 50.0.

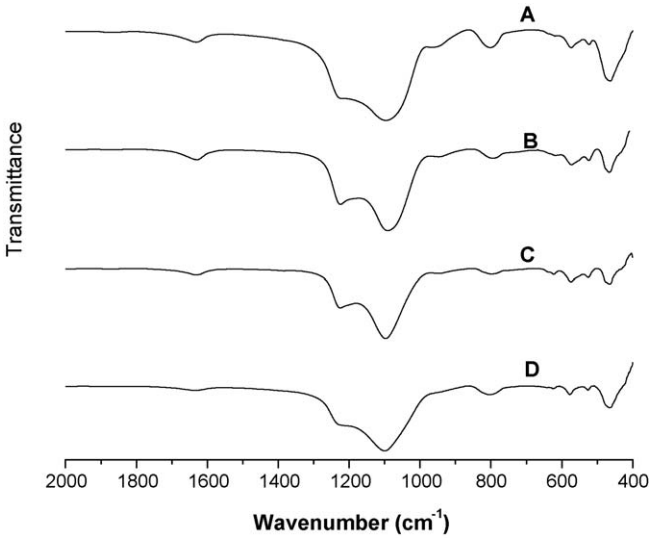

Fig. 4. FTIR spectra of the calcined samples of nanocrystalline zeolite beta catalysts containing different Si/Al ratios: (A) 12.5, (B) 15.0, (C) 25.0 and (D) 50.0.

the intensity of the most intense (302) reflection peak appearing at 22.4° of highly crystalline zeolite beta (Table 1). The crystal sizes obtained by applying Scherrer's equation to (302) reflection peak are in the 20 nm range. Furthermore the high crystallinity of these nanocrystalline zeolite samples can be ascertained from their framework IR spectra (Fig. 4), which show in the 500–650 cm^{-1} region the features characteristic of zeolite beta [20]. The large and broad peak appeared in the range of 1060–1090 cm^{-1} is due to asymmetric stretching vibration ($\upsilon_{a(OTO)}$), which is sensitive to the silicon and aluminum contents in the zeolite framework and it shifts to lower wavenumber with the decrease of Si/Al ratio [29]. The peak appeared at 950 cm^{-1} in the samples of low Si/Al ratio is related to the terminal SiO^{-} groups consequence of small crystallites [13].

^{29}Si NMR spectra (Fig. 5) of as made zeolite beta samples of different Si/Al ratios (A–D) reveal three major overlapping resonances. Those around −113, −114 and −109, −110 ppm are

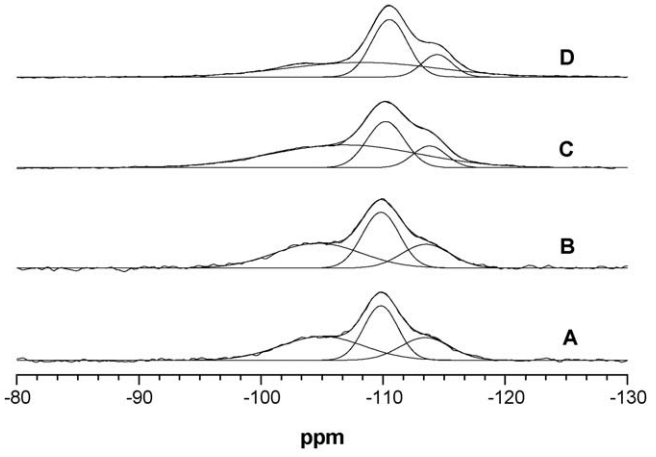

Fig. 5. ^{29}Si NMR spectra of as made nanocrystalline zeolite beta catalysts containing different Si/Al ratios: (A) 12.5, (B) 15.0, (C) 25.0, (D) 50.0 and (ES) extended structures of zeolite beta (Si/Al ratio = 15.0).

assigned as two different types of Si (4Si) sites which are characteristic of this zeolite [21] and the peak at −104 to −105 ppm is assigned as Si (3Si, 1Al) sites. For the higher Si/Al ratios, a large and broad peak around at −107 ppm is assigned to Si(3Si, 1OH) species and this peak hinders the observation of Si(3Si, 1Al) band. No other resonance band is observed in these samples. ^{27}Al NMR spectra of as made zeolite beta samples of A–D show the resonance centered at 52.3 ppm and FWHM around 7 ppm. This chemical shift is typical of Al in $Al(OSi)_4$ tetrahedral environments and no other coordination is observed in as made zeolites. These data confirms the formation of crystalline zeolite beta with different Si/Al ratios.

The binding energies of Si 2p and Al 2p levels vary between 103.5 and 103.7 eV and between 74.5 and 74.9 eV, respectively. These values are close to those reported recently [30] for zeolite beta. The results of the bulk and the surface Si/Al ratios determined by chemical analysis and XPS (Table 1) are in good agreement, which indicate the homogeneity of the samples. The values of auger parameter (α^1) obtained from sum of the binding energy of Al 2p and the kinetic energy of photoelectron resulting from Al KLL peak, for all Si/Al ratios are close to 1460 eV to prove aluminum is in 4-fold coordination.

Fig. 6 presents TEM images of nanocrystalline zeolite beta prepared by SCF crystallization and depressurization of the zeolites containing different Si/Al ratios (Fig. 6A–D). Smaller particles are observed in the samples containing lower Si/Al ratios.

^{13}C NMR analyses of nanocrystalline zeolite catalysts (A–D) show two resonance lines centered at 6 and 52 ppm in all spectra corresponding to carbon atoms of methyl and methylene groups [31]. CHN chemical analyses reveal that the C/N ratio of as made samples is constant at 8. These results indicate that the incorporated TEA cation is intact during the SCF aided crystallization and depressurization.

The TG–DTG profiles (Fig. 7) of as made zeolite beta catalysts provide further support to the formation of zeolite beta with different Si/Al ratios without degradation of template molecules during the SCF crystallization and depressurization. The zeolite beta, when synthesized in the absence of alkaline cations, only the TEA^+ cations are balancing the Al in $Al(OSi)_4^-$ framework positions and SiO^- groups in connectivity defects. Table 2 indicates the weight loss in four regions, which are in the following temperature ranges: (I) 25–150, (II) 150–350, (III) 350–500 and (IV) 500–750 °C. Up to 150 °C there is an endotherm due to the desorption of occluded methanol and toluene, supercritical fluids added during preparation of zeolite beta. In range of 150–350 °C, the major products desorbed are ethylene, triethylamine and carbon dioxide as determined by MS, which indicate the degradation of TEA moieties by Hoffmann elimination reaction and the presence of hydrocarbons (H_c) heavier than ethylene shows some oligomerization followed by rearrangement and cracking of the resulting oligomer occurred at acidic sites. The temperature region II is thus assigned to TEA^+ cations balancing the charge of SiO^- groups in connectivity defects. In this region, the weight loss increases as Si/Al ratio increases. The same products are also detected in third weight loss region (350–500 °C) and the signal intensity increases as Si/Al ratio decreases. The fourth weight loss region corresponds to the burning of organics and signal intensity decreases as Si/Al ratio increases. The high

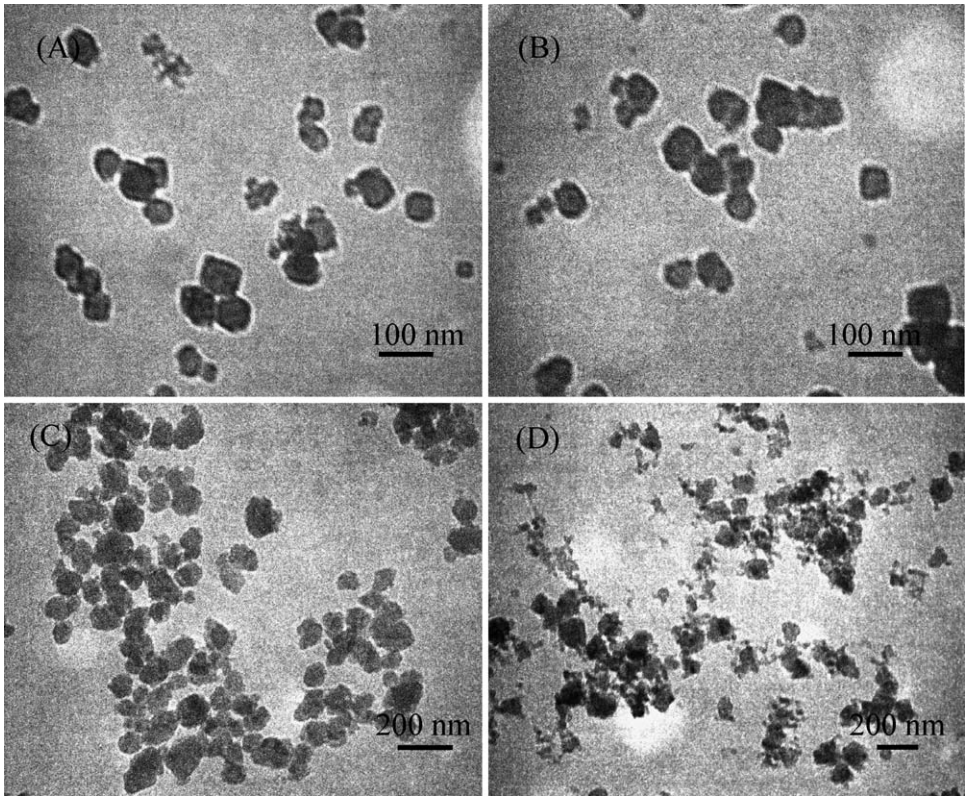

Fig. 6. TEM images of nanocrystalline zeolite beta catalysts containing different Si/Al ratios: (A) 12.5, (B) 15.0, (C) 25.0 and (D) 50.0.

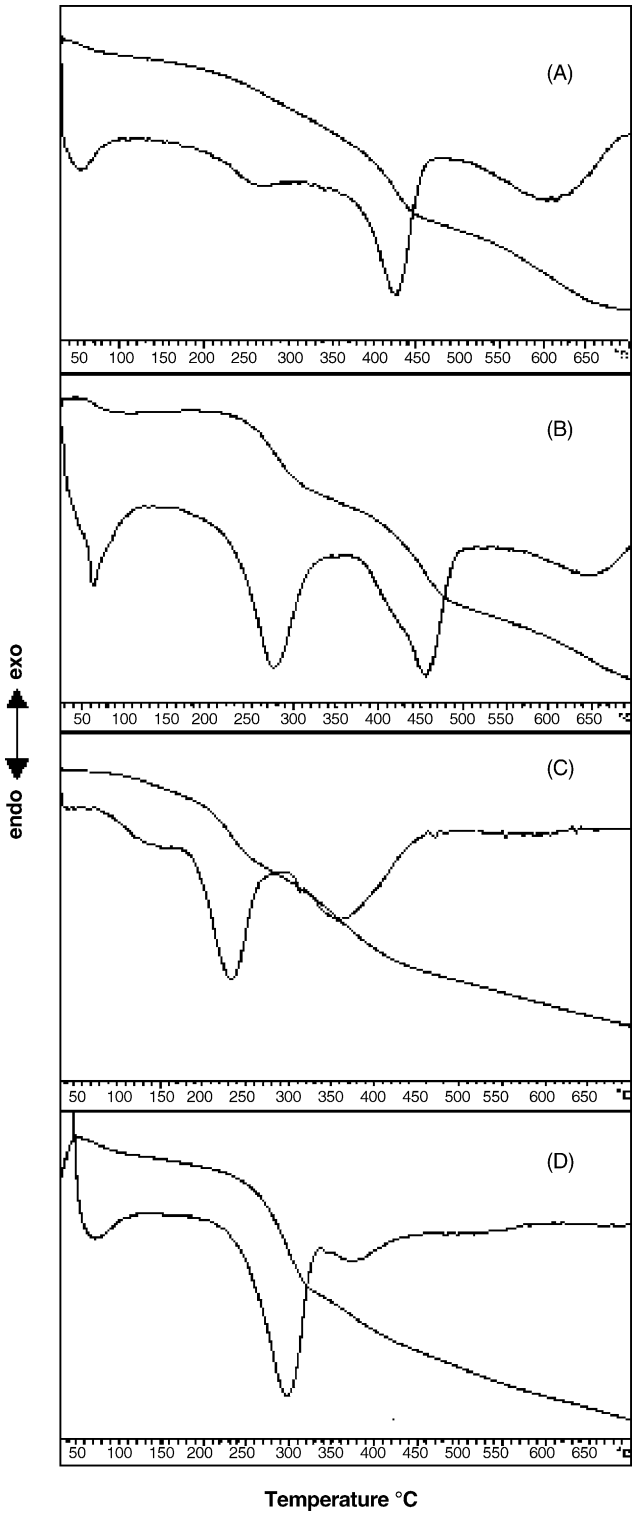

Fig. 7. TGA–DTG profiles of as made nanocrystalline zeolite beta catalysts containing different Si/Al ratios: (A) 12.5, (B) 15.0, (C) 25.0 and (D) 50.0.

temperature regions III and IV are assigned to TEA^+ cations balancing the framework $Al(SiO)_4^-$ species so in this region the weight loss increases as Si/Al ratio decreases.

Temperature-programmed desorption of ammonia (NH_3-TPD) curves exhibits (Fig. 8) three desorption peaks. The peak present between 215 and 225 °C is assigned to weak acidic centers of silanol groups and defect sites. The peak present around 400 °C is due to Bronsted acid sites created by framework aluminum. The third and high temperature shoulder peak at 500 °C is assigned as framework Lewis acidic sites [32]. The amount of ammonia desorbed depends on the Si/Al ratio and it decreases with increasing Si/Al ratio (Table 1).

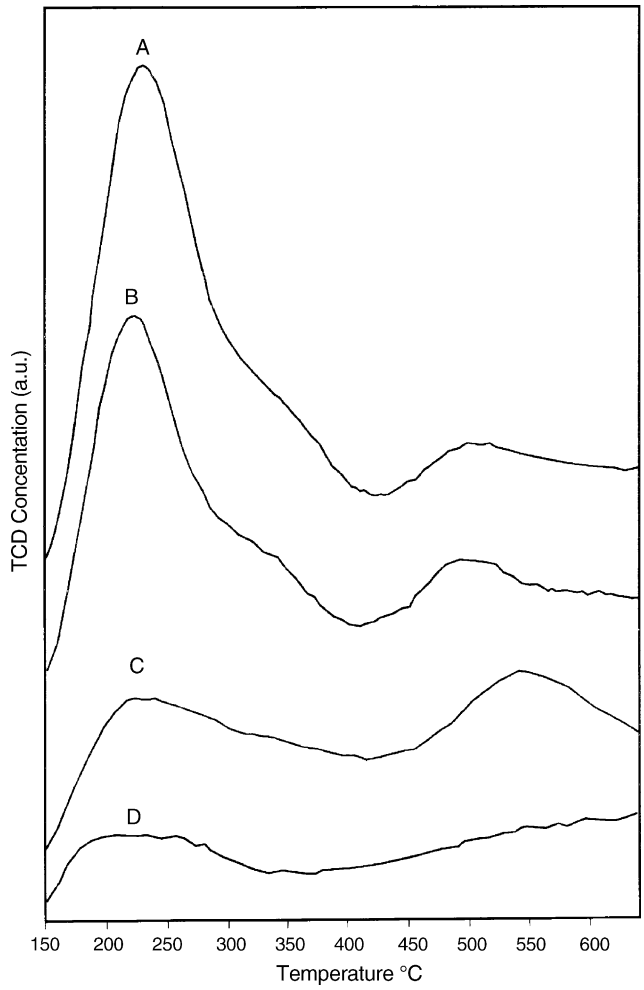

Fig. 8. Temperature-programmed desorption of ammonia (NH_3-TPD) profiles of nanocrystalline zeolite beta catalysts containing different Si/Al ratios: (A) 12.5, (B) 15.0, (C) 25.0 and (D) 50.0.

3.3. Activity of nanocrystalline zeolite beta in nitration of o-xylene

The mononitro derivatives of *o*-xylene isomers are used as intermediates for the production of vitamins, agrochemicals, fragrances and dyes. Although 4- and 3-nitro-*o*-xylenes are useful starting materials for the production of riboflavin (Vitamin B2) and mefenamic acid, an agrochemical, respectively, the former is required in large tonnage. Selective nitration of *o*-xylene, thus, assumes higher importance. Nitration of *o*-xylene in the conventional method, using a mixture of nitric acid and sulfuric acid as the nitrating mixture gives a mixture of 4-nitro-*o*-xylene 31–55% and 3-nitro-*o*-xylene 45–69%. The excellent applications of 4-nitro-*o*-xylene isomer in general and the poor isomeric selectivity towards 4-nitro-*o*-xylene or large amounts

Table 2
Thermogravimetric analysis in air: weight loss (wt%) as a function of temperature

Sample	Signal (temperature)				Total
	I (25–150 °C)	II (150–350 °C)	III (350–500 °C)	IV (500–700 °C)	
A	1.43	5.81	7.95	6.54	21.73
B	0.76	6.92	7.89	5.64	21.21
C	1.53	10.89	4.45	2.86	19.73
D	0.48	11.38	2.80	1.97	16.63

of oxygenates [33] expressed in the nitration of *o*-xylene in the classic nitration reaction in particular prompted us to undertake the present nitration of xylenes using beta zeolite in an effort to evolve eco-friendly and high atom utilization process. In this series we have reported that microcrystalline zeolite beta is an efficient and eco-friendly catalyst for the nitration of *o*-xylene with high regio-selectivity in liquid phase. The reusability of the solid acid catalyst is also being possible by azeotropic removal of water formed in the reaction and present in nitric acid [34].

Nanocrystalline zeolite beta catalysts synthesized by SCF aided crystallization are tested for the nitration of *o*-xylene and these catalysts showed good activity and higher selectivity than the microcrystalline zeolite beta catalysts. The results are given in Table 3. Among the catalysts studied, A containing Si/Al = 12.5 is more active. The higher activity of the nanocrystalline zeolite beta catalysts can be attributed to the fact that the presence of small crystals containing large external surface area and also the presence of the higher number of acidic sites.

Moreover nanocrystalline zeolite beta catalysts (Si/Al ratios: 12.5–50) display consistently higher selectivity towards 4-nitro-*o*-xylene (Fig. 9). The selectivities are quite impressive over the microcrystalline zeolite beta. The higher selectivity of the nano zeolites is attributed to the fast diffusion enabling the reaction inside the pores of zeolite. This result is in consonance to the earlier observation [35]. The reusability of nanocrystalline zeolite A was tested for 5 cycles. Consistent activities were observed but selectivity towards 4-nitro-*o*-xylene decreased slightly (Table 3).

Table 3
Nitration of *o*-xylene using different zeolite beta catalysts

Catalyst	Conversion (wt%)	4-/3- ratio
Blank	20.0	0.93
Microcrystalline zeolite beta II[a]	42.0	2.27
Microcrystalline zeolite beta I[a]	20.0	1.54
HT 15	32.0	1.31
A		
First cycle	54.5	3.29
Fifth cycle	53.0	3.20
B	52.5	2.96
C	34.7	2.92
D	32.2	2.82

Reaction conditions: 100 mg of catalyst, 10 mmol of *o*-xylene, 12 mmol of 70% HNO_3, 6 ml of dichloroethane under reflux, and stirring for 5 h.

[a] SiO_2/Al_2O_3 ratio: microcrystalline zeolite beta II = 22, microcrystalline zeolite beta I = 27 and reaction time 4 h.

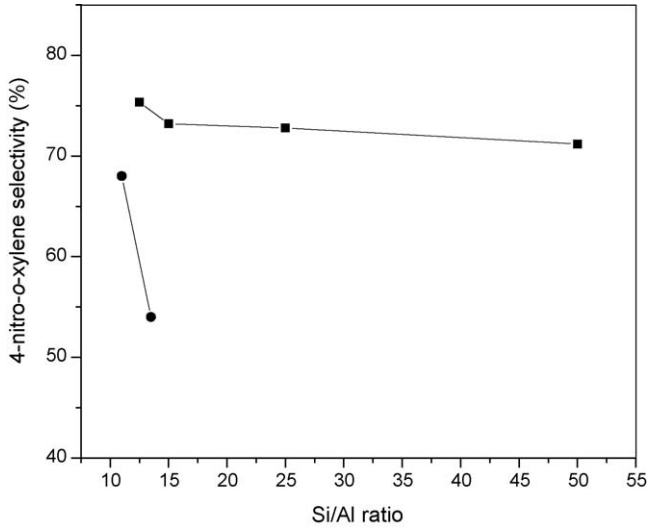

Fig. 9. Nitration of *o*-xylene using different zeolite beta catalysts as a function of Si/Al ratio (■) conversion, (●) selectivity of 4-nitro-*o*-xylene (reaction conditions: 100 mg of catalyst, 10 mmol of *o*-xylene, 12 mmol of 70% HNO_3, 6 ml of dichloroethane under reflux, and stirring for 5 h).

Zeolite beta obtained by high temperature treatment and in absence of supercritical fluids (HT 15) is also tested for the nitration reaction. Low conversions and selectivities are observed (Table 3), which can be ascribed to the presence of non-porous large particles.

4. Conclusions

In conclusion, nanocrystalline zeolite beta catalysts with different Si/Al ratios are prepared by hydrothermal treatment coupled with SCF aided crystallization. The use of supercritical fluids in the preparation method further provides quantitative yields of nanocrystalline zeolite beta in shorter crystallization time and dispensing with the general protocols adopted for the separation of zeolites. The obtained nanocrystalline zeolite beta is thoroughly characterized by various techniques. XRD, IR, TEM and MAS NMR analyses of the intermediate structures of nanocrystalline zeolite beta demonstrates the influence of supercritical conditions on the rate of crystallization and provides better understanding on the formation of nanocrystalline zeolite beta. The obtained nanocrystalline zeolite beta samples show good conversions and high selectivity towards 4-nitro-*o*-xylene in nitration of *o*-xylene.

Acknowledgments

We wish to thank the CSIR for financial support under the NMITLI project. B.P.C.R. thanks the Council of Scientific and Industrial Research (CSIR), India, for the award of Senior Research Fellowship.

References

[1] H.H. Kung, M.C. Kung, Appl. Catal. A: Gen. 246 (2003) 193.
[2] G.A. Somorjai, Y.G. Bordko, Catal. Lett. 76 (2001) 1.
[3] (a) A. Corma, J. Catal. 216 (2003) 298;
(b) L. Tosheva, V.P. Valtchev, Chem. Mater. 17 (2005) 2494.
[4] J.C. Jansen, E.J. Creyghton, S.L. Njo, H. van Koningsveld, H. van Bekkum, Catal. Today 38 (1997) 205.
[5] P. Botella, A. Corma, J.M. Lopez-Nieto, S. Valencia, R. Jacquot, J. Catal. 195 (2000) 161.
[6] M.A. Camblor, A. Corma, A. Martinez, V. Martinez-Soria, S. Valencia, J. Catal. 179 (1998) 537.
[7] E.G. Derouane, I. Schmidt, H. Lachas, C.J.H. Christensen, Catal. Lett. 95 (2004) 13.
[8] F.D. Renzo, Catal. Today 41 (1998) 37.
[9] S. Mintova, N.H. Olson, V. Valtcev, T. Bein, Science 283 (1993) 958.
[10] N.B. Castagnola, P.K. Dutta, J. Phys. Chem. B 102 (1998) 16996.
[11] B.J. Schoeman, J. Sterte, J.E. Otterstedt, Zeolites 14 (1994) 110.
[12] P.R. Hari Prasad Rao, M. Matsukata, Chem. Comm. (1996) 1441.
[13] M.A. Camblor, A. Corma, A. Mifsud, J. Perez-Pariente, Stud. Surf. Sci. Catal. 105 (1997) 341.
[14] P.E. Savage, S. Gopalan, T.I. Mizan, C.J. Martino, E.E. Brock, AIChE J. 41 (1995) 1723.
[15] A. Baiker, Chem. Rev. 99 (1999) 453.
[16] K.J. Klabunde, J. Sark, O. Koper, C. Mohs, D.G. Park, S. Decker, Y. Jiang, I. Lagadie, D. Zhang, J. Phys. Chem. 100 (1996) 12142.
[17] S. O'Neil, R. Mokaya, M. Poliakoff, J. Am. Chem. Soc. 124 (2002) 10637.
[18] T.S. Zemanian, G.E. Fryxell, J. Liu, S. Mattigod, J.A. Franz, Z. Nie, Langmuir 17 (2001) 8172.
[19] Y. Liu, T.J. Pinnavaia, J. Am. Chem. Soc. 125 (2003) 2376.
[20] J. Perez-Pariente, J.A. Martens, P.A. Jacobs, Appl. Catal. 31 (1987) 35.
[21] M.A. Camblor, A. Corma, S. Valencia, Micropor. Mesopor. Mater. 25 (1998) 59.
[22] R. Mostowicz, F. Testa, F. Crea, R. Aillo, A. Fonseca, J.B. Nagy, Zeolites 18 (1997) 308.
[23] J. Perez-Pariente, J.A. Martens, P.A. Jacobs, Zeolites 8 (1988) 46.
[24] R. Kumar, A. Bhaumik, R.K. Ahedi, S. Ganapathy, Nature 381 (1996) 298.
[25] G. Pope, Micropor. Mesopor. Mater. 21 (1998) 333.
[26] Q. Li, B. Mihailova, D. Creaser, J. Sterte, Micropor. Mesopor. Mater. 43 (2001) 51.
[27] A. Tuel, Chem. Mater. 11 (1999) 1865.
[28] (a) M.K. Diedrich, F.G. Klarner, J. Am. Chem. Soc. 120 (1998) 6212;
(b) M.K. Diedrich, D. Hochstrate, B. Jimmy, F.G. Klarner, Angew. Chem., Int. Ed. Engl. 33 (1994) 1079.
[29] C. Yang, Q. Xu, J. Chem. Soc. Faraday Trans. 93 (1997) 1675.
[30] F. Collignon, P.A. Jacobs, P. Grobet, G. Poncelet, J. Phys. Chem. B 105 (2001) 6812.
[31] E. Bourgeat-Lami, F.D. Renzo, F. Fajula, P.H. Mutin, T.D. Courieres, J. Phys. Chem. 96 (1992) 3807.
[32] G.H. Kuehl, H.K.C. Timken, Micropor. Mesopor. Mater. 35–36 (2000) 521.
[33] K. Smith, A. Musson, G.A. DeBoos, J. Org. Chem. 63 (1998) 8448.
[34] M.L. Kantam, B.M. Choudary, N.S. Kumar, K.V. Ramprasad, J. Mol. Catal., A Chem. 229 (2005) 67.
[35] S. Bernasconi, G.D. Pirngruber, R. Prins, J. Catal. 224 (2004) 297.